HHS Public Access

Author manuscript

Biochem Biophys Res Commun. Author manuscript; available in PMC 2020 January 29.

Published in final edited form as:

Biochem Biophys Res Commun. 2019 January 29; 509(1): 69–75. doi:10.1016/j.bbrc.2018.12.059.

Identification of myosin II as a cripto binding protein and regulator of cripto function in stem cells and tissue regeneration

Malachia Hoover[a,2], **Farhana Runa**[a], **Evan Booker**[c], **Jolene K. Diedrich**[b], **Erika Duell**[a], **Blake Williams**[a], **Caroline Arellano-Garcia**[a,2], **Toni Uhlendorf**[a], **Sa La Kim**[a], **Wolfgang Fischer**[c], **James Moresco**[b], **Peter C. Gray**[c,1], **Jonathan A. Kelber**[a,*]

[a]Department of Biology, California State University Northridge, USA

[b]Mass Spectrometry Core, The Salk Institute for Biological Studies, USA

[c]Clayton Foundation for Peptide Biology, The Salk Institute for Biological Studies, USA

Abstract

Cripto regulates stem cell function in normal and disease contexts via TGFbeta/activin/nodal, PI3K/Akt, MAPK and Wnt signaling. Still, the molecular mechanisms that govern these pleiotropic functions of Cripto remain poorly understood. We performed an unbiased screen for novel Cripto binding proteins using proteomics-based methods, and identified novel proteins including members of myosin II complexes, the actin cytoskeleton, the cellular stress response, and extracellular exosomes. We report that myosin II, and upstream ROCK1/2 activities are required for localization of Cripto to cytoplasm/membrane domains and its subsequent release into the conditioned media fraction of cultured cells. Functionally, we demonstrate that soluble Cripto (one-eyed pinhead in zebrafish) promotes proliferation in mesenchymal stem cells (MSCs) and stem cell-mediated wound healing in the zebrafish caudal fin model of regeneration. Notably, we demonstrate that both Cripto and myosin II inhibitors attenuated regeneration to a similar degree and in a non-additive manner. Taken together, our data present a novel role for myosin II function in regulating subcellular Cripto localization and function in stem cells and an important regulatory mechanism of tissue regeneration. Importantly, these insights may further the development of context-dependent Cripto agonists and antagonists for therapeutic benefit.

Keywords

Cripto; Actomyosin signaling; Stem cells; Tissue regeneration; Proteomics; Zebrafish

[*]Corresponding author. Department of Biology, California State University Northridge, Northridge, CA, 91330, USA. jonathan.kelber@csun.edu (J.A. Kelber).

[1]Present address: ScienceMedia Inc.

[2]Present address: Stanford University.

Appendix A. Supplementary data

Supplementary data to this article can be found online at https://doi.org/10.1016/j.bbrc.2018.12.059.

1. Introduction

Cripto (Cripto-1, TDGF1) is a GPI-anchored glycoprotein and the founding member of the epidermal growth factor-Cripto-1-FRL-1-Cryptic (EGF-CFC) family of vertebrate signaling proteins. First isolated as a potential oncoprotein in human and mouse teratocarcinoma cells [1–3], Cripto is now recognized as a critical regulator of developmental and tumorigenic signaling via multiple growth factor and mitogenic pathways [2–4]. The ER chaperone glucose regulated protein 78 kDa (GRP78) was identified as a Cripto binding partner and cell surface mediator of Cripto signaling [5–7].

In the mouse, Cripto has been detected prior to gastrulation in the 4-day blastocyst and is required for primitive streak formation, patterning of the anterior/posterior axis, specification of mesoderm and endoderm during gastrulation, and establishment of left/right (L/R) asymmetry of developing organs [8]. In addition to being a well-known marker and promoter of the undifferentiated state in normal embryonic and adult stem cells [9–11], Cripto is also aberrantly expressed at high levels in several malignancies [12], where it has been demonstrated to contribute to disease progression [13,14].

Nonetheless, uncertainty remains about Cripto's role in various contexts and the mechanisms that control its pleiotropic functions [4]. This has hindered the development of effective therapies for targeting Cripto in the context of normal stem cell biology or cancer progression. We reasoned that a more comprehensive knowledge of the Cripto interactome could clarify Cripto signaling pathways and functions.

We have used proteomics and identified 51 Cripto binding proteins from human epithelial cells. Bioinformatics analysis of this network revealed regulators of extracellular exosomes, myosin II complexes, and the cytoskeleton. We subsequently found that myosin II activity regulates subcellular localization of Cripto in epithelial and mesenchymal stem cell populations and that myosin II and the zebrafish Cripto ortholog, one-eyed pinhead (oep), function cooperatively to promote wound healing *in vivo*.

2. Results

2.1. Cripto interactome analysis reveals actomyosin-rich network

We previously reported on Cripto signaling and function using the human mammary epithelial cell line MCF10A that was stably transduced with an empty vector or Flag-tagged Cripto-containing vector [5]. As shown in Fig. 1A, we used this cellular model to immunoprecipitate (IP) Flag-Cripto from total cell lysates. Flag antibody immune complexes were analyzed by mass spectrometry (MS) and compared to the respective total cell lysate proteomes (Supplemental Fig. 1) from both cell populations. Proteins that were Flag IP enriched by 2-fold or more in Flag-Cripto cells relative to vector cells across two independent MS runs and which did not change significantly in the total cell lysates were classified as robust Cripto-binding proteins (see Supplemental Data Files 1 and 2 – T1–3).

Using the DAVID Bioinformatics Resource database (v. 6.8) [15,16], we next clustered the 51 Cripto-binding proteins into biological process, cellular component and molecular

function gene ontologies (GO) (Fig. 1B–D and Supplemental Data File 1 – T2–4). Cripto-binding proteins associated with cellular cytoskeleton and myosin II complex GOs included myosin IIs, actins, tubulins, actinins and tropomyosins (Supplemental Data File 1 – T2–4). Total cell lysate proteins enriched or depleted by Cripto overexpression only overlapped with the extracellular exosome GO (Supplemental Figs. 1A–C, Supplemental Data File 1 – T3 and Supplemental Data File 2 – T2–7) suggesting that Cripto may regulate both the trafficking and composition of exosomes.

We next used the Agilent Literature Search plugin in Cytoscape (v. 3.6.0) to generate a Cripto interactome from these 51 Cripto-binding proteins. In addition to 27 of the initial 51 search terms, this interactome contained an additional 149 proteins (Fig. 1E). This interactome was enriched for Akt, Actin, MAPK3 and MYH14 nodes with the highest number of connecting neighbors. Interestingly, Akt was also a central node in the interactome for proteins enriched in the total protein lysates from Cripto-overexpressing MCF10A cells (Supplemental Fig. 1D). The interactome for proteins depleted in the total protein lysates from Cripto-overexpressing MCF10A cells (Supplemental Fig. 1E) contained TP53 as the primary node with the highest number of neighboring connections.

2.2. Myosin II and cripto interact to mediate intracellular localization of cripto and its release from the plasma membrane

To validate the Myosin II/Cripto interaction, MCF10A Vector or Flag-Cripto cell lysates were subjected to Flag IP/Western blotting for MYH9 together with immunofluorescence/confocal co-localization studies. MYH9 was significantly enriched in the IP samples from the Flag-Cripto cells, indicating MYH9 is a Cripto interacting protein (Fig. 2A). Further, observation of endogenous Cripto and MYH9 co-localizing in peripheral cytoplasmic puncta of mesenchymal stem cells (MSCs) strongly supports our identification of myosin IIs as Cripto-interacting proteins (Fig. 2B).

Since Myosin II proteins have been shown to play a role in trafficking proteins from the ER-Golgi network to the cell membrane [17], we hypothesized that Cripto (a GPI-anchored protein) may be shuttled to the plasma membrane and prepared for subsequent GPI-anchor cleavage in a Myosin II-dependent manner. To rule out the possibility that Myosin II elicits this effect on Cripto indirectly by shuttling a GPI-anchor-cleaving factor to the extracellular side of the plasma membrane [18], we first used an intact cell surface TMB-based ELISA assay to quantify levels of Cripto tethered to the cell membrane. In both the MCF10A mammary epithelial Cripto overexpression and endogenous C3H10T1/2 MSC models, we observed that Myosin II inhibition significantly reduced cell surface levels of Cripto (Fig. 2C–D). To evaluate whether Myosin II and upstream ROCK1/2 activities (ROCK1/2 potentiates Myosin II function [19]) simply regulate the subcellular localization of Cripto or whether Cripto co-localization with Myosin II complexes may also require Myosin II activity, we further evaluated endogenous Cripto/Myosin II co-localization in C3H10T1/2 MSCs using confocal microscopy. While Myosin II inhibition did not affect localization of MYH9, it did shift Cripto from being predominantly cytoplasmic/membrane localized to having an enrichment within the perinuclear region (Fig. 2E). Alternatively, ROCK1/2 inhibition caused a shift toward perinuclear localization for both Cripto and MYH9 (Fig.

2E). To test whether GPI anchor-cleaved/soluble levels of Cripto are also regulated by Myosin II activity, we performed immunoblotting on lysates and conditioned media from MCF10A Vector and Flag-Cripto or C3H10T1/2 cells following treatment of cells with a Myosin II inhibitor. While found that GRP78 expression is primarily restricted to the cell lysates, we observed that Cripto is shed into the conditioned media of MCF10A Flag-Cripto cells in a Myosin II-dependent manner (Fig. 2F). Interestingly, while Cripto can be modestly detected in the conditioned media of C3H10T1/2 cells after longer conditioning time points, the shedding effect is much less dependent upon Myosin II activity (Fig. 2G). Nonetheless, these data suggest that Myosin II complexes regulate the subcellular localization of Cripto in both epithelial and mesenchymal cell types.

2.3. Cripto/myosin II signaling promotes stem cell proliferation and is required for tissue regeneration in vivo

To test the functional significance of Cripto on MSC proliferation, we treated C3H10T1/2 cells with soluble Cripto and analyzed cell viability and cell cycle profile. Notably, Cripto treatment stimulated viability of these cells (Fig. 3A) and increased the number of cells in the S-phase of the cell cycle (Fig. 3B). To compare the expression pattern of Cripto and select stem/progenitor cell and non-stem cell markers in primary mammalian systems, we referenced RNA-seq data from a recent study [20] in which murine MSCs were treated either with maintenance (MSC) or bone differentiating (MSC-Bone) médias. Expression levels of Cripto and the mouse orthologs of msxb (MSX3) and ptcl (PTCH1) decrease upon MSC bone differentiation and, as expected, levels of the osteoblast marker sp7 increased during bone differentiation (Fig. 3C).

Since blastemal stem cell expansion and/or dedifferentiation during zebrafish (Danio rerio) caudal fin regeneration marks a critical period of stem cell activity [21,22], we sought to isolate and observe the migratory behavior of this cell population *ex vivo* (Supplemental Fig. 2A and Supplemental Movies 1 and 2). In parallel, we measured the time-dependent expression patterns of oep and established markers of progenitor blastemal cells (msxb), scleroblasts (ptc1) and osteoblasts (sp7) post-amputation of the zebrafish caudal fin. The highest expression levels of these markers occur at the 96 hpa time point (Fig. 3D) [23]. As expected, peak expression of differentiated cell type markers including endothelium (fli1 a) and melanocytes (tryp1b) did not correlate with that of the progenitor cell markers. By contrast, the peak expression pattern of oep correlated with that of the progenitor cell markers (Fig. 3D).

Supplementary video related to this article can be found at https://doi.org/10.1016/j.bbrc.2018.12.059.

We next used the juvenile zebrafish tail bud regeneration model to test the role of oep (Cripto) and myh9l1/2 (MYH9/10) during wound repair. ALK4^{L75A}-Fc (L75A-Fc) is a point-mutant and Fc-chimeric derivative of the Cripto-binding ALK4 extracellular domain (ECD) that blocks Cripto-dependent stem cell expansion [6,24]. To support our previous work establishing inter-species functionality of the L75A-Fc reagent, the ALK4 binding residues in mouse and human Cripto are conserved in zebrafish oep (Supplemental Fig. 2B). L75A-Fc treatment of regenerating tail bud tissue in juvenile zebrafish inhibited tissue

regrowth by nearly 50% (Fig. 3E). Conversely, the addition of soluble Cripto significantly stimulated regrowth and this effect was blocked by the L75A-Fc reagent (Fig. 3E). We next asked whether Cripto/oep-dependent zebrafish caudal fin regeneration could be further antagonized by Myosin II inhibition. Similar to the Cripto inhibitor, the Myosin II inhibition reduced regrowth by ~50% (Fig. 3F). Notably, cotreatment with both inhibitors had approximately the same effect as treatment with either inhibitor alone. The fact that these inhibitors were not additive *in vivo* suggests that Myosin II and Cripto/oep may function together or in an overlapping pathway.

3. Discussion

Herein, we have evaluated the functional significance of a novel Cripto-Myosin II interaction in the context of mesenchymal stem cells and an *in vivo* model of tissue regeneration. Myosin II proteins represent two of the 51 Cripto interacting proteins identified in this study (Fig. 1). We further validate this interaction using biochemistry and immunofluorescence in Cripto overexpression and endogenous cell systems (Fig. 2A–B). Notably, we demonstrate that Myosin II function is required for intracellular transport of Cripto (Fig. 2C–G). Finally, we demonstrate that Myosin II and Cripto function cooperatively during stem cell proliferation *in vitro* and stem cell mediated tissue regeneration *in vivo* (Fig. 3).

In this regard, Myosin II proteins have been previously reported to play roles in cell proliferation/survival, intracellular trafficking and cell migration, [25–27]. Furthermore, these functional patterns have also been observed more broadly for the entire actomyosin system [28,29], including the upstream regulator Rho kinase (ROCK1/2) [30]. These previous observations are consistent with our newly identified role for Myosin II in regulating Cripto localization and function (Figs. 2 and 3). It will be important for future studies to evaluate the role of Myosin II-dependent cell surface versus soluble Cripto functions in regulating these phenotypes.

It is interesting to note that the Cytoscape interactome generated from Cripto binding proteins was enriched for Akt, Actin, MAPK3 and MYH14 nodes having the highest number of connecting neighbors. Furthermore, we find that GRP78 is a common interactor of both Akt and Actin (Fig. 1E). These findings are consistent with previous studies demonstrating a role for Cripto in activating mitogenic Akt and MAPK signaling pathways in a GRP78-dependent manner [5,10], as well as GRP78 regulating PI3K/Akt signaling functions in a Cripto-independent fashion [31]. Nonetheless, questions remain as to what governs Cripto’s ability to selectively regulate Akt and whether this effect depends in part on both Myosin II and/or GRP78 proteins.

Finally, while the total cellular levels of Cripto were relatively equal (as analyzed by Western blot and immunofluorescence) between our overexpression MCF10A and endogenous C3H10T1/2 cell systems, we observed striking differences between the amount of Cripto released into the conditioned media between these two systems (Fig. 2F–G) with the overexpression MCF10A system releasing abundantly more soluble Cripto. However, we also observed that modulation of cell surface Cripto in the overexpression MCF10A system

was much less sensitive to Myosin II inhibition (Fig. 2C–D) as compared to cell surface levels of Cripto in the endogenous C3H10T1/2 cells. Future work should evaluate the functional relevance of these differences.

4. Experimental procedures

4.1. Cell lines

MCF10A and C3H10T1/2 cells were obtained from the American Tissue Culture Collection (ATCC) and were cultured in accordance with ATCC recommendations.

4.2. Cell lysates and Co-immunoprecipitation

Cell lysates were prepared in radioimmunoprecipitation assay (RIPA) buffer as previously described [1]. Protein extracts were precleared for 2 h at 4 °C and bound/eluted to/from anti-FLAG M2 beads in accordance with manufacturer's protocol.

4.3. Mass spectrometric analysis

Mass-specific bands were excised from a Coomasie-stained protein gel. Destained gel slices were treated with 100 ng trypsin in 10 μl ammonium bicarbonate solution (20 mM) at 37 °C for 16 h. Samples were dried after mixing 1 μl of the supernatant spotted onto a matrix-assisted laser desorption ionization target and 1 μl of a saturated solution of alpha-cyano-hydroxycinnamic acid. A Bruker Ultraflex TOF/TOF (Bruker Daltonics, Billerica, MA) mass spectrometer was used for sample analysis. Mass fingerprint data were analyzed from two or more runs.

4.4. Bioinformatics methods of cripto binders and exosome enrichment

Cripto binding proteins and Cripto upregulated/downregulated proteins were analyzed for Gene Ontology (GO) using the DAVID database. Interactome analysis was performed using Cytoscape 3.0 and the Agilent Literature Search plugin.

4.5. Western blot

Cells were treated with vehicle control or blebbistatin prior to collecting cell lysates or conditioned media for Western blotting (WB). Proteins were probed with indicated antibodies with the following dilutions: Anti-Flag (Salk Institute, 1:400), Cripto (Salk Institute, 1:400), α-tubulin (cell signaling, 1:1000), GRP78 (Salk Institute, 1:1000) and MYH9 (ThermoFisher, 1:100). Secondary antibodies were used at 1:5000 dilutions.

4.6. Immunofluorescence/confocal imaging

C3H10T1/2 cells were plated and treated with indicated inhibitors for 8 h prior to fixing and staining for MYH9 (Thermo-Fisher, 1:400) and Cripto (Salk Institute, 1:400) and appropriate fluorescently-conjugated secondary antibody (ThermoFisher, 1:400). Images were captured at 100X magnification using the Leica TCS SP5 II confocal microscope with a 150 μm pinhole and 10-frame average.

4.7. Measurement of cell surface expression of cripto

MCF10A and C3H10T1/2 cells were plated and stained for an intact cell ELISA using indicated antibodies as previously described [1].

4.8. Zebrafish amputations and regrowth quantification

AB strain zebrafish were maintained at 28 °C on a 14/10 h light/dark cycle and fed twice daily. For Juvenile Zebrafish amputation, 6 dpf frys were anesthetized in a 0.005% (w/v) solution of Tricaine diluted in E3 media for no longer than 3 min. The caudal fin was then amputated using a surgical blade underneath a stereoscope at 20X magnification. Frys were transferred into a petri dish of fresh E3 media to recover. Once recovered, frys were placed in 1 mL of E3 media in a 24-well plate at 1 fry per well. The 0 h time point of amputation was imaged at 80X magnification (SteREO Lumar.V12, Carl Zeiss, Jena, Germany) and treated with indicated treatments. The regrowth after postamputation was imaged again at 80X magnification. Using Fiji, the 24-h regrowth was quantified.

For the adult, zebrafish were anesthetized in 50 mL of aquatic system water into a 0.02% solution (w/v) solution of Tricaine for no longer than 3 min. Zebrafish were placed underneath a stereoscope (AO Spencer Stereo Microscope) at 20X magnification and the caudal fin was then amputated using a surgical dissection blade. The initial amputation and subsequent regrowth tissues were collected at the indicated time points after the initial amputation in RNeasy Mini Kit lysis buffer (Qiagen, Netherlands). Samples were flash frozen and stored at −20 °C for further use.

4.9. Zebrafish RNA harvest, cDNA synthesis and qPCR

For RNA isolation, tissue samples were microhomogenized according to Claremont BioSolutions, Upland, CA). cDNA synthesis was performed using the Maxima Universal First Strand Kit (Thermo Scientific, Grand Island, NY). Both RNA and cDNA were quantified by using Nanodrop 2000c Spectrophotometer (Thermo Scientific, Grand Island, NY). Quantitative PCR (qPCR) was performed by using Maxima SYBR Green/ROX qPCR Master Mix using a 7300 Fast Real-Time PCR System (Applied Biosystems, Waltham, MA).

4.10. Pharmacological studies in juvenile zebrafish

Frys were treated in 500uL/well in a 24-well plate using for each treatment with Cripto inhibitor, ALK-4/L75A-Fc (5 μg/mL) and control IgG (5 μg/mL), and a Myosin II inhibitor, Blebbistatin (5 μg/mL) and DMSO as a control. Conditioned media were collected from 90% confluent MCF10A Vector or Flag-Cripto. Cells grown for 72 h and the conditioned media were centrifuged at 1000 rpm for 5 min and supernatant were collected and applied to frys at 500uL/well.

4.11. Random 2-D migration

Digested primary blastemal tissue from wounded adult zebrafish caudal fins were plated in a tissue culture treated in a 24-well plate. Media were changed after 24 h and several x,y-coordinates were selected for time-lapse phase-contrast imaging at 10X magnification.

4.12. Aqueous one cell viability assay

C3H10T1/2 cells were plated in complete media in a 96-well plate. After 24 h soluble Cripto derived from conditioned media of the MCF10A Flag-Cripto and Vehicle control were applied to the cells. The Aqueous One Assay was performed in accordance with the manufacturer's protocol.

4.13. Cell cycle analysis

C3H10T1/2 cells were grown in a 6-well plate and after 24 h, conditioned media from MCF10A Flag-Cripto cells and Vehicle control were added to the cells. Cell cycle analysis was performed as previously described [4].

4.14. Statistical analyses

Student t-test or one-way ANOVA w/post-test analyses were used to evaluate statistical significance between sample populations. Data presented are representative of three biological replicates.

Supplementary Material

Refer to Web version on PubMed Central for supplementary material.

Acknowledgements

We are grateful to members of the Kelber laboratories for their contributions to manuscript assembly, editing and revision. Funding was provided by the CSUN College of Science and Math, Medtronic/Minimed, the Sidney Stern Memorial Trust, Dr. Gary and Vera Sutter and NIH 5SC1GM121182 award (to J.A.K.); NIH NIGMS 5R25GM063787 (to M.Y.H. via M.E.Z.); NIH NIGMS 5RL5GM118975 (to E.D. via C.L.S.), and the Clayton Foundation for Peptide Biology (to P.C.G. and W.F.)

References

[1]. Ciardiello F, Dono R, Kim N, et al., Expression of cripto, a novel gene of the epidermal growth factor gene family, leads to in vitro transformation of a normal mouse mammary epithelial cell line, Cancer Res 51 (1991) 1051–1054. [PubMed: 1846316]

[2]. Schier AF, Neuhauss SC, Helde KA, et al., The one-eyed pinhead gene functions in mesoderm and endoderm formation in zebrafish and interacts with no tail, Development 124 (1997) 327–342. [PubMed: 9053309]

[3]. Shen MM, Schier AF, The EGF-CFC gene family in vertebrate development, Trends Genet 16 (2000) 303–309. [PubMed: 10858660]

[4]. Klauzinska M, Castro NP, Rangel MC, et al., The multifaceted role of the embryonic gene Cripto-1 in cancer, stem cells and epithelial-mesenchymal transition, Semin. Canc. Biol 29 (2014) 51–58.

[5]. Kelber JA, Panopoulos AD, Shani G, et al., Blockade of Cripto binding to cell surface GRP78 inhibits oncogenic Cripto signaling via MAPK/PI3K and Smad2/3 pathways, Oncogene 28 (2009) 2324–2336. [PubMed: 19421146]

[6]. Spike BT, Kelber JA, Booker E, et al., CRIPTO/GRP78 signaling maintains fetal and adult mammary stem cells ex vivo, Stem Cell Reports 2 (2014) 427–439. [PubMed: 24749068]

[7]. Shani G, Fischer WH, Justice NJ, et al., GRP78 and Cripto form a complex at the cell surface and collaborate to inhibit transforming growth factor beta signaling and enhance cell growth, Mol. Cell Biol 28 (2008) 666–677. [PubMed: 17991893]

[8]. Ding J, Yang L, Yan YT, et al., Cripto is required for correct orientation of the anterior-posterior axis in the mouse embryo, Nature 395 (1998) 702–707. [PubMed: 9790191]

[9]. Gershon E, Hadas R, Elbaz M, et al., Identification of trophectoderm-derived Cripto as an essential mediator of embryo implantation, Endocrinology 159 (4) (2018 4 1) 1793–1807. [PubMed: 29506220]

[10]. Miharada K, Karlsson G, Rehn M, et al., Cripto regulates hematopoietic stem cells as a hypoxic-niche-related factor through cell surface receptor GRP78, Cell Stem Cell 9 (2011) 330–344. [PubMed: 21982233]

[11]. Park SW, Do HJ, Han MH, et al., The expression of the embryonic gene Cripto-1 is regulated by OCT4 in human embryonal carcinoma NCCIT cells, FEBS Lett 592 (2018) 24–35. [PubMed: 29223130]

[12]. Strizzi L, Mancino M, Bianco C, et al., Netrin-1 can affect morphogenesis and differentiation of the mouse mammary gland, J. Cell. Physiol 216 (3) (9 2008) 824–834. [PubMed: 18425773]

[13]. Zoni E, Chen L, Karkampouna S, et al., CRIPTO and its signaling partner GRP78 drive the metastatic phenotype in human osteotropic prostate cancer, Oncogene 36 (2017) 4739–4749. [PubMed: 28394345]

[14]. El-Sayed IY, Daher A, Destouches D, et al., Extracellular vesicles released by mesenchymal-like prostate carcinoma cells modulate EMT state of recipient epithelial-like carcinoma cells through regulation of AR signaling, Cancer Lett 410 (2017) 100–111. [PubMed: 28935391]

[15]. Huang DW, Sherman BT, Tan Q, et al., The DAVID Gene Functional Classification Tool: a novel biological module-centric algorithm to functionally analyze large gene lists, Genome Biol 8 (2007) R183. [PubMed: 17784955]

[16]. Huang DW, Sherman BT, Tan Q, et al., DAVID Bioinformatics Resources: expanded annotation database and novel algorithms to better extract biology from large gene lists, Nucleic Acids Res 35 (2007) W169–W175. [PubMed: 17576678]

[17]. Bedi D, Dennis JC, Morrison EE, et al., Regulation of intracellular trafficking and secretion of adiponectin by myosin II, Biochem. Biophys. Res. Commun 490 (2017) 202–208. [PubMed: 28606474]

[18]. Watanabe K, Bianco C, Strizzi L, et al., Growth factor induction of Cripto-1 shedding by glycosylphosphatidylinositol-phospholipase D and enhancement of endothelial cell migration, J. Biol. Chem 282 (2007) 31643–31655. [PubMed: 17720976]

[19]. Kreutzman A, Colom-Fernandez B, Jimenez AM, et al., Dasatinib reversibly disrupts endothelial vascular integrity by increasing non-muscle myosin II contractility in a ROCK-dependent manner, Clin. Canc. Res 23 (2017) 6697–6707.

[20]. Meyer MB, Benkusky NA, Sen B, et al., Epigenetic plasticity drives adipogenic and osteogenic differentiation of marrow-derived mesenchymal stem cells, J. Biol. Chem 291 (2016) 17829–17847. [PubMed: 27402842]

[21]. Akimenko MA, Johnson SL, Westerfield M, et al., Differential induction of four msx homeobox genes during fin development and regeneration in zebrafish, Development 121 (1995) 347–357. [PubMed: 7768177]

[22]. Zou J, Beermann F, Wang J, et al., The Fugu tyrp1 promoter directs specific GFP expression in zebrafish: tools to study the RPE and the neural crest-derived melanophores, Pigm. Cell Res 19 (2006) 615–627.

[23]. Nechiporuk A, Keating MT, A proliferation gradient between proximal and msxb-expressing distal blastema directs zebrafish fin regeneration, Development 129 (2002) 2607–2617. [PubMed: 12015289]

[24]. Kelber JA, Shani G, Booker EC, et al., Cripto is a noncompetitive activin antagonist that forms analogous signaling complexes with activin and nodal, J. Biol. Chem 283 (2008) 4490–4500. [PubMed: 18089557]

[25]. Arora S, Saha S, Roy S, et al., Role of nonmuscle myosin II in migration of wharton's jelly-derived mesenchymal stem cells, Stem Cell. Dev 24 (2015) 2065–2077.

[26]. Zhang C, Lee HJ, Shrivastava A, et al., Long-term in vitro expansion of epithelial stem cells enabled by pharmacological inhibition of PAK1-ROCK-myosin II and TGF-beta signaling, Cell Rep 25 (2018) 598–610, e595. [PubMed: 30332641]

[27]. Crish J, Conti MA, Sakai T, et al., Keratin 5-Cre-driven excision of nonmuscle myosin IIA in early embryo trophectoderm leads to placenta defects and embryonic lethality, Dev. Biol 382 (2013) 136–148. [PubMed: 23911870]

[28]. Vogler G, Liu J, Iafe TW, et al., Cdc42 and formin activity control non-muscle myosin dynamics during Drosophila heart morphogenesis, J. Cell Biol 206 (2014) 909–922. [PubMed: 25267295]

[29]. Dix CL, Matthews HK, Uroz M, et al., The role of mitotic cell-substrate adhesion Re-modeling in animal cell division, Dev. Cell 45 (2018) 132–145 e133. [PubMed: 29634933]

[30]. Hu Y, Hu D, Yu H, et al., Hypoxiainducible factor 1alpha and ROCK1 regulate proliferation and collagen synthesis in hepatic stellate cells under hypoxia, Mol. Med. Rep 18 (2018) 3997–4003. [PubMed: 30132575]

[31]. Hsu HS, Liu CC, Lin JH, et al., Involvement of ER stress, PI3K/AKT activation, and lung fibroblast proliferation in bleomycin-induced pulmonary fibrosis, Sci. Rep 7 (2017) 14272. [PubMed: 29079731]

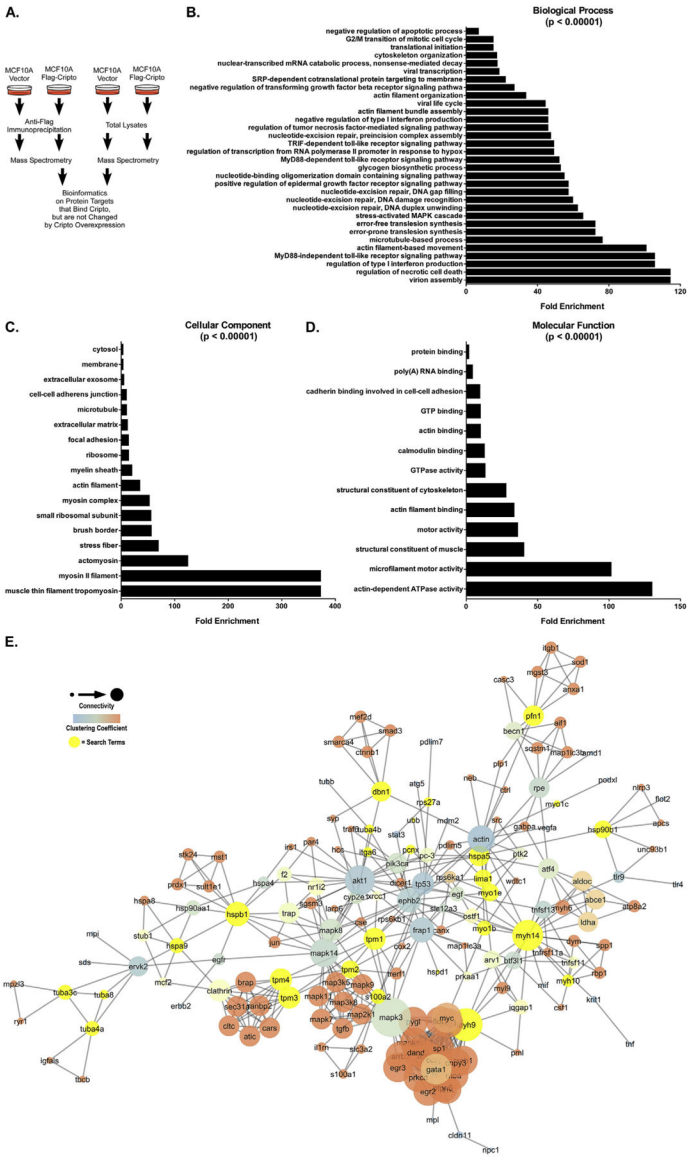

Fig. 1. Cripto interactome analysis reveals actomyosin-rich network

A. Schematic representation of MCF10A Vector or Flag-Cripto cell lysate and anti-Flag immunoprecipitation (IP) for Cripto. B-D. DAVID database gene ontology enrichment for biological processes, cellular components and molecular functions within the set of 51 Cripto-binding proteins. E. Cytoscape Agilent Literature Search generated interactome networks of Cripto-binding proteins.

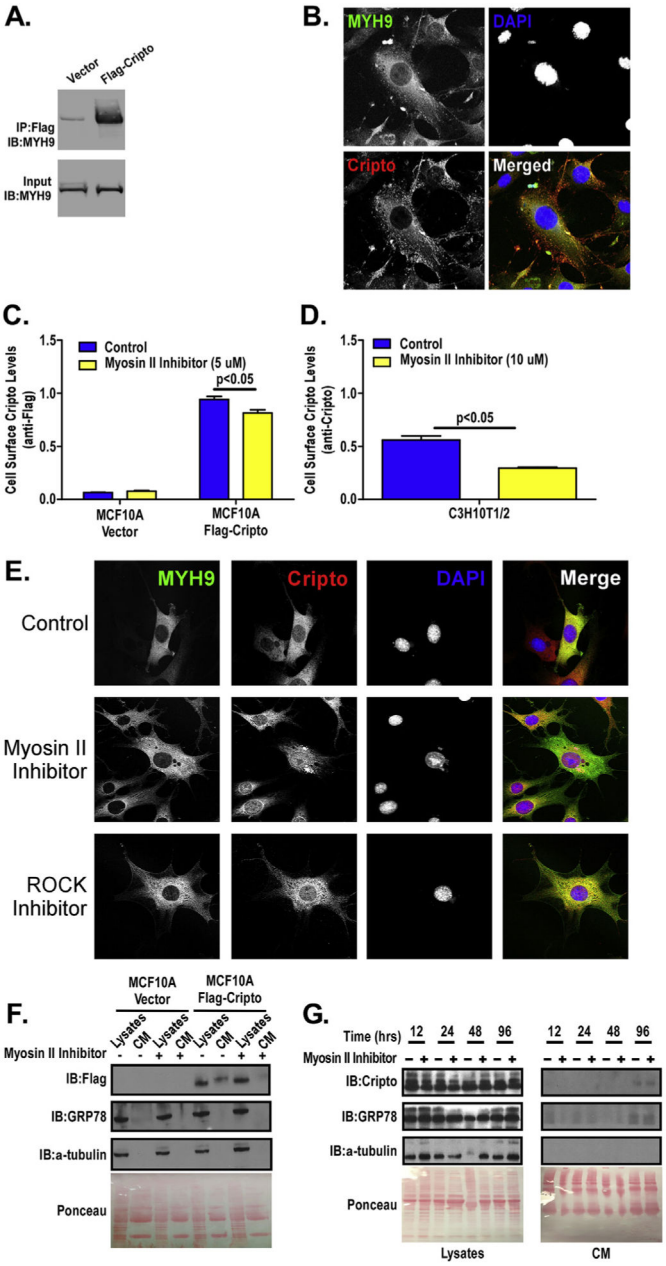

Fig. 2. Myosin II and Cripto interact to mediate intracellular localization of Cripto and its release from the plasma membrane

A. Immunoprecipitation/Western blot analysis of Myosin IIA (MYH9) from MCF10A Vector and Flag-Cripto cells. B. Confocal microscopy analysis of MYH9 and Cripto co-localization in murine C3H10T1/2 MSC at 100X magnification. C-D. Cell surface analysis of Cripto using an intact cell ELISA assay in MCF10A Vector/Flag-Cripto or C3H10T1/2 cells, respectively. Myosin II inhibitor, blebbistatin used at the indicated dose. E. Confocal microscopy analysis of MYH9 and Cripto localization in murine C3H10T1/2 MSCs (63X magnification) treated with either Myosin II inhibitor or ROCK inhibitor. F-G.Western blot analysis of either Flag-tagged (F) or endogenous (G) Cripto in cell lysates and conditioned media (CM) produced from MCF10A Vector/Flag-Cripto or C3H10T1/2 cells, respectively.

Myosin II inhibitor, blebbistatin, was used at 10 μM. Alpha-tubulin and ponceau stains were used to assess loading control in lysates and CM samples, respectively.

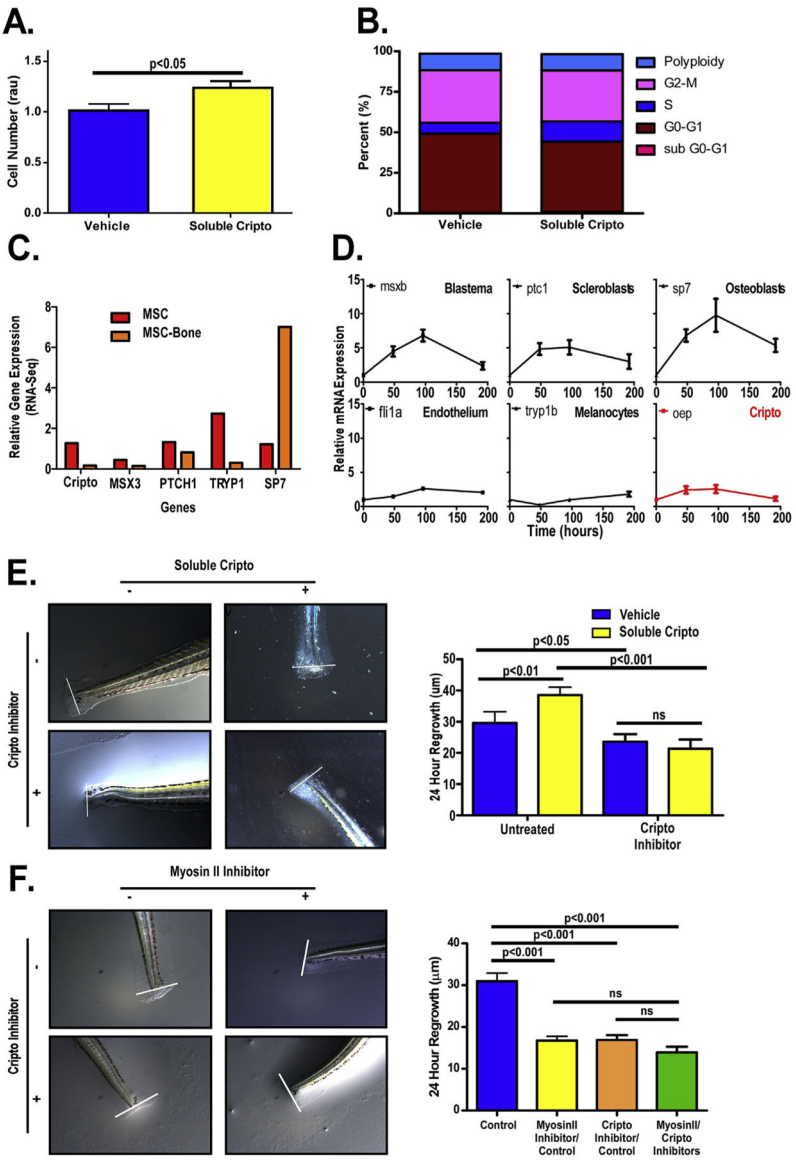

Fig. 3. Cripto/Myosin II signaling promotes stem cell proliferation and is required for tissue regeneration *in vivo*

A. Cell proliferation/survival of C3H10T1/2 cells treated with vehicle (MCF10A Vector) or soluble Cripto (MCF10A Flag-Cripto) conditioned media was measured using AQueous One assay. B. Cell cycle analysis using propidium iodide staining in C3H10T1/2 cells. C. RNA-seq data representing progenitor/differentiation markers and Cripto gene expression in mesenchymal stem cells (MSCs) treated with normal or bone differentiating (MSC-bone) media (Meyer et al., 2016 JBC). D. QPCR analysis of progenitor/differentiation markers and Cripto (one-eyed pinhead, oep) expression in the regenerating zebrafish caudal fin at the indicated time points post-amputation. E. Left panel, images of control and Cripto inhibitor treated juvenile zebrafish tails in combination with vehicle (MCF10A Vector) or soluble Cripto (MCF10A Flag-Cripto) conditioned media at 48 h post amputation (hpa). Right panel, average 24 h mean regrowth (um) of amputated zebrafish tails treated as in left panel. F. Left panel, images of control and Cripto/Myosin II inhibitor treated juvenile zebrafish

tails. Right panel, average 24 h mean regrowth (um) of amputated zebrafish tails treated as in left panel.